RSC Advances

PAPER

Cite this: *RSC Adv.*, 2022, **12**, 6025

Designing bimetallic zeolitic imidazolate frameworks (ZIFs) for aqueous catalysis: Co/Zn-ZIF-8 as a cyclic-durable catalyst for hydrogen peroxide oxidative decomposition of organic dyes in water

Osama Abuzalat, *[a] Hesham Tantawy, [a] Mustafa Basuni,[b] Mohamed H. Alkordi [b] and Ahmad Baraka[a]

Received 12th January 2022
Accepted 11th February 2022

DOI: 10.1039/d2ra00218c

rsc.li/rsc-advances

ZIF-8 is well known hybrid material that is self-assembled from inorganic and organic moieties. It has several potential applications due to its unique structure. One of these potential applications is in advanced oxidation processes (AOP) *via* a heterogeneous catalysis system. The use of modified ZIF-8/H_2O_2 for the destruction of the azo dye methyl orange (MO) is presented in this work to explore its efficacy. This work presents the bimetallic Co/Zn-ZIF-8 as an efficient catalyst to promote H_2O_2 oxidation of the MO dye. Co/Zn-ZIF-8 was synthesized through a hydrothermal process, and the pristine structure was confirmed using XRD, FTIR, and XPS. The Co/Zn-ZIF-8/H_2O_2 system successfully decolorized MO at the selected pH 6.5. It was found that more than 90% of MO (10 ppm) was degraded within only about 50 minutes. Proposed radical and redox mechanisms are presented for H_2O_2 decomposition where the redox mechanism is suggested to predominate *via* a Co(II)/Co(III) redox consecutive cyclic process.

1. Introduction

Zeolitic imidazolate frameworks (ZIFs) represent a particular class of coordination polymers that are built from metal ion nodes and methyl-imidazolate (MIM) linkers. ZIFs are crystalline solids possessing structures analogous to aluminosilicate zeolites with an intrinsic permanent porosity and considerable thermal and chemical stability.[1,2] Due to the many desirable characteristics of this class of microporous solids, ZIFs were heavily explored within the last decade for applications such as gas separation, adsorption (gas and liquid phases), sensing[3] electronic devices, drug delivery, and catalysis.[4,5]

Indeed, applying ZIFs for heterogeneous catalysis has been systematically investigated and has covered several approaches such as degradation of some dyes/organics (*e.g.*, methylene blue and indigo carmine) *via* photocatalysis[6] catalytic synthesis of some organic derivatives (styrene carbonates),[7] hydrogen generation,[8] CO_2 conversion,[9] Knoevenagel condensation,[10] Friedel–Crafts acylation,[11] trans-esterification,[12] and monoglyceride synthesis.[13] Although reductive catalytic degradation of some dyes was previously investigated by the ZIF-8/$NaBH_4$ catalysis system,[14] or adsorption by ZSM-5 zeolite[15] utilization of ZIFs for the counter-redox direction, the oxidative catalytic degradation of organic contaminants (heterogeneous catalysis employing the oxidant H_2O_2), to best of our knowledge has not previously been reported. This scarcity of in-depth investigations into the catalytic activity of ZIFs for oxidative degradation of organic dyes did not allow for critical evaluation of ZIFs in many environmental applications, one of which is the efficient oxidative remediation of wastewater.

In this work, the known bimetallic Co/Zn-ZIF-8 has been selected for oxidative catalysis degradation primarily due to its significant hydrolytic stability in aqueous solutions, a decisive factor for any material to utilize in aqua-degradation systems.[6] Synthesis and characterization of Co/Zn-ZIF-8 are presented, especially detailed XPS analysis. The rate and kinetic-modelling of oxidative catalytic degradation of the stable dye methyl orange by Co/Zn-ZIF-8/H_2O_2 system are presented as well. To the best of our knowledge, this is the first report presenting the activity of a bimetallic ZIF-8 for degrading a synthetic dye *via* catalytic H_2O_2 decomposition.

2. Experimental

2.1 Materials

All chemicals were of analytical grade and have been used without further purification: 2-methylimidazole (2-MIM, 99%, Sigma-Aldrich), triethylamine (TEA, 99%, Alfa Aesar), zinc acetate dihydrate ($Zn(CH_3CO_2)_2 \cdot 2H_2O$, 98%, Sigma Aldrich),

[a]*Department of Chemical Engineering, Military Technical College, Cairo, Egypt. E-mail: osama.abuzalat@mtc.edu.eg*

[b]*Center for Materials Science, Zewail City of Science and Technology, Giza 12578, Egypt*

cobalt nitrate hexahydrate ($Co(NO_3)_2 \cdot 6H_2O$, 98%, Sigma Aldrich), acetone (98%, VWR), and deionized water (DI water).

2.2 Co/Zn-ZIF-8 synthesis

The bimetallic Co/Zn-ZIF-8 was synthesized hydrothermally. The molar ratio of cobalt nitrate and zinc acetate was 0.5 : 0.5 and the molar ratio of metal salts and 2-MIM was 1 : 1. Typically, $Co(NO_3)_2 \cdot 6H_2O$ (0.176 g, 0.5 mmol) and $Zn(CH_3CO_2)_2 \cdot 6H_2O$ (0.109 g, 0.5 mmol) were separately dissolved in DI water (10 ml). Another solution was prepared by dissolving 2-MIM (0.082 g, 1 mmol) in a mixture of DI water (10 ml) and TEA (2 ml). Subsequently, the Zn(II) and Co(II) solutions were mixed and magnetically stirred for 15 minutes. The mix-solution was poured into 2-MIM solution under magnetic stirring. A purple suspension was gradually formed which was then heated in an oven (80 °C) for 6 h. Thereafter, the violet solid was partially settled and collected by centrifugation (6000 rpm, 15 min), washed with acetone, water (3 times × 10 ml), and finally dried in an oven at 80 °C overnight.

In addition, two ZIF-8 control samples were also prepared, each was based on a single metal ion, Zn-ZIF-8 and Co-ZIF-8. It was found that while Zn-ZIF-8 was hydro-stable, Co-ZIF-8 readily degraded in hydrogen peroxide solution.

2.3 Co/Zn-ZIF-8 characterization

The chemical structure of Co/Zn-ZIF-8 was explored *via* FTIR analysis (KBr pellet method using Jasco FT/IR 4100). For its crystalline nature, powder X-ray diffraction (PXRD, Shimadzu XD-l) was applied. SEM/EDX analysis (Zeiss EVO-10 microscopy) was utilized to study the surface morphology and to acquire more information about elemental composition. The X-ray photoelectron spectrum of Co/Zn-ZIF-8 (XPS-Thermo Fisher Scientific, USA) was acquired with a monochromatic Al-K_α (1486.7 eV). BET analysis (N_2 adsorption, NOVA Station A) was also performed to determine surface area.

2.4 MO degradation

Three MO solutions (250 ml each with adjusted initial pH at 6.5) of different initial concentrations, 2, 5 and 10 ppm, were used to examine MO degradation rate by adding Co/Zn-ZIF-8 (0.05 g) and H_2O_2 (1 ml (45% H_2O_2, 0.5 mM)) for each. With no agitation or shacking, the three samples were left in dark at ambient temperature (≈27 °C). The darkness condition was applied to avoid the probable photocatalysis that may happen due to lab stray lights. Periodically, every 10 minutes, about 3 ml from each sample were withdrawn to measure the absorbance of MO remnants using UV-Vis spectrophotometer (Jasco Model 7850 at $\lambda = 591$ nm). The dosage effect was also considered by using different amounts of Co/Zn-ZIF-8, 0.01, 0.025, 0.05, and 0.1 g, keeping other conditions the same as previous.

It is important to mention that the selection of pH 6.5, near neutral, was decided to avoid probable metal ion leaching from Co/Zn-ZIF-8 structure by acidity and to avoid possible hydrolysis by alkalinity.[16] In addition, such selection is appropriate to circumvent Co/Zn-ZIF-8 surface interaction with acidity or alkalinity, because of the probable buffering MIM moieties, which might affect H_2O_2-produced oxidative species.[17,18] In addition, the decomposition rate of H_2O_2 by Co/Zn-ZIF-8 was monitored and recorded by the traditional triiodide-Ghormley method.[19,20]

3. Results and discussion

3.1 Co/Zn-ZIF-8 characterization before and after MO degradation

Fig. 1(A) shows the SEM image of Co/Zn-ZIF-8 crystals before and after 5 cycles of catalysis. The crystals morphology can be sought as of dodecahedron type of similar average sizes, about 0.4 μm. This shape is conventional to most of the ZIF-8 samples.[3] Some deterioration in morphology has been noticed after 5 cycles. This may be due to the harsh condition by using H_2O_2.

Fig. 1(B) shows the FTIR spectra of two Co/Zn-ZIF-8 samples: the before degradation sample (BE-S) and the after 5 degradation-cycles sample (AF-S). For both spectra, the vibrations recorded in the range 760–1422 cm^{-1} are attributed to the 2-MIM ring. Also, for both spectra, the characteristic band at 1585 cm^{-1} arose from C=N stretching vibration while the peaks at 2800–3100 cm^{-1} correspond to the aliphatic and aromatic stretching C–H of 2-MIM, respectively. The broad peak around 3400 cm^{-1} could be assigned to adsorbed moisture from the atmosphere into the ZIF crystals, with spikes that can be associated with the N–H stretching vibration of the residual 2-MIM. The very similarity of these spectra indicates the chemical stability of Co/Zn-ZIF-8 against H_2O_2, especially the organic part.

XRD patterns of BE-S, AF-S, and the simulation are shown in Fig. 1(C). These patterns are almost identical which verifies the successful preparation of Co/Zn-ZIF-8 as a ZIF-8 material with a body-centred cubic crystal lattice structure.[21] Specifically, the similarity of BE-S and AF-S patterns validates its crystalline robustness against H_2O_2. Hence, it can be suggested that the incorporation of cobalt does not alter the topology of the framework structure and the original topology was retained due to: (i) the similarity of the ionic size of cobalt and zinc (Co^{2+} 0.79 Å and Zn^{2+} 0.74 Å) and (ii) the similarity of coordination number for the Co(II) and Zn(II) ions in this framework structure.[22]

Fig. 1(D) presents the N_2-adsorption isotherms of BE-S and AF-S and the accordingly determined BET surface areas are 1210 and 255 $m^2\ g^{-1}$ respectively. The obvious reduction in the surface area could be referred to as the adsorption of degradation products of MO which does not affect the successive degradation cycles as will be shown later.

Fig. 2 presents the XPS survey spectra of Co/Zn-ZIF-8 samples, BE-S (A) and AF-S (B). The presence of the principal Co 2p, Zn 2p, N 1s, C 1s, and O 1s core levels before and after degradation with relatively similar abundances proposes the significant chemical stability of Co/Zn-ZIF-8 during H_2O_2 decomposition process. Table 1 indicates that pristine Co/Zn-ZIF-8 suffered a slight degradation due to the 5-cycles of degradation where a significant increase in oxygen abundance was recorded. Moreover, the observed similarities of atomic ratios of Co/Zn and C/N before and after H_2O_2 treatment

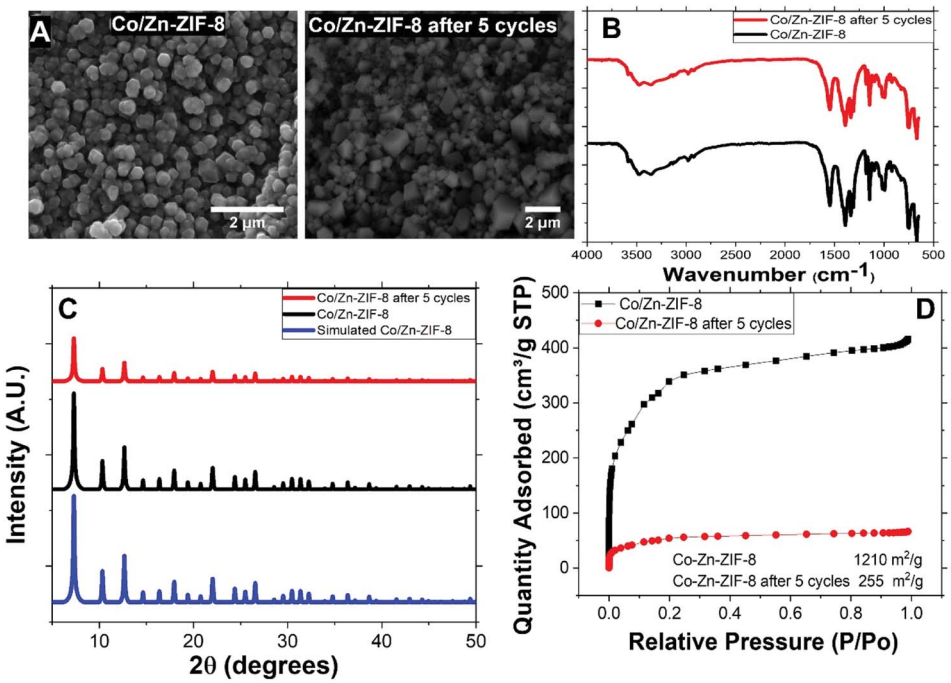

Fig. 1 (A) SEM of Co/Zn-ZIF-8, (B) FTIR of BE-S and AF-S, (C) XRD patterns of BE-S and AF-S, and (D) N_2 adsorption isotherm and BET surface area of BE-S and AF-S.

confirms the successive H_2O_2-decomposition without any significant change in the chemical composition of Co/Zn-ZIF-8.

Further, in-depth analysis concerning the XPS results was carried out to investigate the possible effects of H_2O_2 treatment on Co/Zn-ZIF-8 structure and to assist the understanding of the decomposition mechanism.

Fig. 3(A and B) presents Co 2p high-resolution XPS spectra of BE-S and AF-S. Two main peaks are present for both samples. These peaks are indexed to a spin–orbit splitting of Co $2p_{3/2}$ and $2p_{1/2}$ at 781.16 and 797.08 eV respectively for BE-S and 781.28 and 797.27 eV for AF-S respectively. The two peaks of BE-S are very similar to those of AF-S which indicate the chemical stability of Co/Zn-ZIF-8. The splitting energies of the 2p doublet ($\Delta = 2p_{1/2} - 2p_{3/2}$) for both samples were found to be close and equal to about 16 eV, which is quite similar to the literature.[23,24]

Deconvoluting cobalt Co $2p_{3/2}$ and Co $2p_{1/2}$ spectra present two main peaks under each one along with their significant corresponding satellites peaks. The fitted peak at 780.96 eV (BE-S) is very similar to the peak at 781.04 eV (AF-S) and the fitted peak at 783.16 eV (BE-S) is also very similar to the peak at 783.3 eV (AF-S). These peaks should be attributed mainly to Co $2p_{3/2}$ of Co^{2+}/Co^{3+} mixed valency.[24–29] Further, the observed peaks around 797.03 eV (BE-S) and 797.1 eV (AF-S) and 799.19 (BE-S) and 800.82 eV (AF-S) could be also attributed to Co $2p_{1/2}$ of Co^{2+}/Co^{3+} mixed structure.[30–33] Accordingly, both oxidation states, Co^{2+} and Co^{3+}, are always present within Co/Zn-ZIF-8 structure before and after H_2O_2 treatment which also indicates the reasonable stability of the chemical structure of the pristine sample.

Co $2p_{3/2}$ satellite peaks are observed at 786.33 (BE-S) and 786.66 eV (AF-S) and 789.36 (BE-S) and (AF-S) 789.95 eV.[26,34,35]

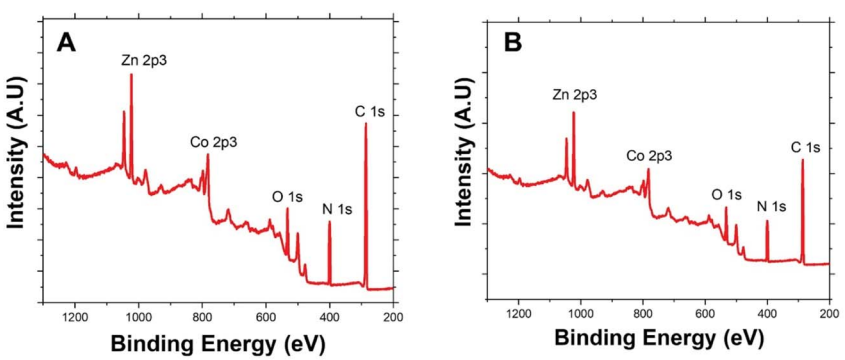

Fig. 2 XPS survey spectra of Co/Zn-ZIF-8: (A) BE-S and (B) AF-S.

Table 1 Relative atomic abundances of elemental composition; BE-S and AF-S

Sample		Co	Zn	N	C	O
BE-S	Atomic wt%	3.1%	3.7%	28.6%	54.4%	10.3%
	Relative abundance to Co ions	1.0	1.2	9.3	17.7	3.3
AF-S	Atomic wt%	2.9%	3.3%	27.1%	52.0%	14.7%
	Relative abundance to Co ions	1.0	1.1	9.2	17.6	5.0

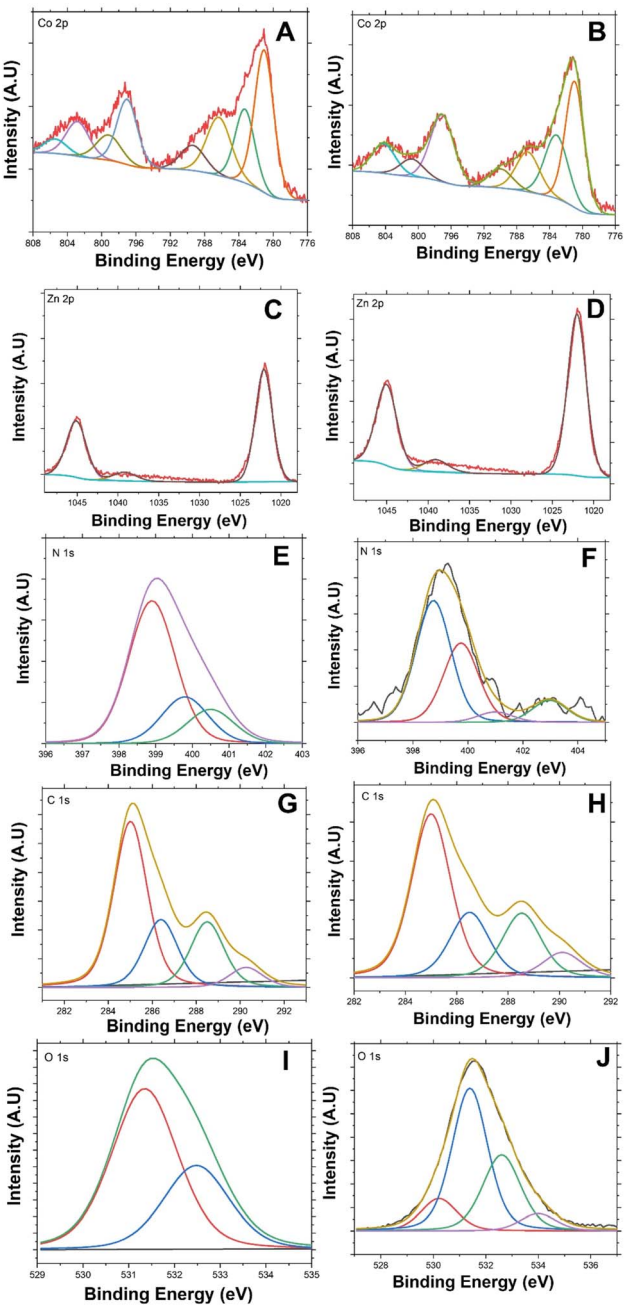

Fig. 3 XPS detailed line scans of the Co/Zn-ZIF-8 for BE-S (left column) and AF-S (right column): (A and B) Co 2p peak, (C and D) Zn 2p peak, (E and F) N 1s peak, (G and H) C 1s peak, and (I and J) O 1s peak.

Also, Co $2p_{1/2}$ satellite peaks are observed at 805.1 (BE-S) and 804.69 eV (AF-S) in addition to another one at 802.82 (AF-S) which also supports the possibility of having a stable Co^{2+}/Co^{3+} mixed structure before and after H_2O_2 treatment.[27,36–38] The disappearance of the satellite peaks at 802.82 eV after H_2O_2 treatment may indicate the possibility of having a slight difference within the electronic environment and charge transfer around Co^{2+}/Co^{3+} after H_2O_2 decomposition.[39–41]

Recalling that cobalt precursor was divalent, however, it seems that some Co^{2+} ions have been oxidized to Co^{3+} during synthesis.[34,42,43] This depiction confirms that cobalt ions should have a different coordination environment,[44–46] which subsequently allows consecutive redox electron transfer.[45,47,48] In addition, the presence of a mixed metal system, such as the present case (Zn/Co), rises the metal-heterogeneity mode of the mixed valence system that should enhance the redox activity a character that is essential for catalytic reactions.[49,50]

Fig. 3(C and D) presents the $2p_{3/2}$ and $2p_{1/2}$ lines for Zn^{2+} for both BE-S and AF-S which are assigned at 1022.02 and 1045.03 eV for BE-S and 1022.09 and 1045.1 eV for BE-S and AF-S, respectively. The binding-energy difference between these lines is about 23.0 eV and they are free from multiple splitting and other complicating effects.[51–53] A distinct weak peak located at 1039.09 eV (BE-S) and 1039.2 eV (AF-S) is observed, which may be due to the modulation of binding energies arising from some ligand dissimilarities of Zn^{2+} ions.[53–55] The existence of some Co^{3+} nods, in addition to Zn^{2+} and Co^{2+} nods, throughout Co/Zn-ZIF-8 structure must be balanced with the negative anion (COO^-) available within the reaction medium. This phenomenon may induce some local dipole moments at Co^{3+} sites influencing spots of higher surface energies.[53,56,57]

Fig. 3(E and F) presents N 1s core-level spectra of the Co/Zn-ZIF-8 for both BE-S and AF-S. They are resolved into multiple peaks for different nitrogen environments. The de-convolutions were decomposed into three (BE-S) and four (AF-S) peaks respectively. The most intense N 1s peak at 398.8 eV (BE-S) and 398.91 eV (AF-S) could be attributed to the pyridinic nitrogen atoms.[58–62] Because of the little difference between the binding energy of the metal-coordinated N and pyridinic N,[59,63] this peak indicates the successful coordination through nitrogen-sp^2 bonding with metal nods.[59,63,64] In addition, it also designates that most reacted methylimidazole should exist as methyl imidazolate.[65,66]

Here are some important observations to comment on which reveals some side effect of H_2O_2 on Co/Zn-ZIF-8 structure. The pyrrolic peak of nitrogen is observed at 399.75 eV (BE-S) and at

399.83 eV (AF-S).[58,59,61,62] The peak intensity increased after H_2O_2 treatment which could imply some partial consumption of the pyridinic species. Also, the intensity of N-graphitic[58,59,62,67] protonated pyrrolic[68] peak at 400.5 eV (BE-S) has been diminished, at 401.11 eV (AF-S), due to repetitive oxidation. On the other hand, a weak peak around 402.95 eV representing the oxidized N (pyridine-N-oxide) species[67–69] appears for (AF-S). This new peak is of higher energy concerning N-pyridinic due to relatively stronger electron localization associated with poorer conjugation at sp^3-bonded sites. Hence, lower charge mobility is expected to lead to only a minor decline in degradation performance.[70,71] These results propose a minor oxidative deterioration of the Co/Zn-ZIF-8 after five successive oxidation cycles with a survivable and stable structure.

Fig. 3(G and H) presents the de-convoluted C 1s spectra. Each consisted of four main peaks for both (BE-S) and (AF-S). These peaks are observed at 285.13, 286.57, 288.44, and 289.97 eV for BE-S and at 284.90, 286.26, 288.46, and 290.11 eV for AF-S which can be assigned to C–C/C=C,[61,72,73] C=N,[74–76] C–N[61,76,77] and C=O,[78–80] respectively.

The presence C=O species, even with low abundance, confirms the possibility of incorporation of acetate anion within the structure as it was mentioned previously. It is obvious that there are no significant changes within the de-convoluted C 1s due to H_2O_2 treatment, and this suggests that Co/Zn-ZIF-8 chemical structure withstands H_2O_2 oxidative medium to an acceptable extent. However, the cautious analysis showed a slight relative decrease in C=N abundance with respect to that of C–N after H_2O_2 treatment. This observation agrees with the decrease of pyridinic-N with respect to pyrrolic-N after H_2O_2 treatment. Furthermore, C=O peak showed a diminutive increase after H_2O_2 treatment, at 290.11 eV, which was expected due to possible minor oxidation of trace pyridinic units to form pyridone species integrated within Co/Zn-ZIF-8 structure.[81,82]

Fig. 3(I and J) presents the de-convoluted O 1s spectra. Although the relative abundance of oxygen is low with respect to other elemental compositions, specifically C and N, the O 1s core-level de-convoluted seems to be very interesting. The O 1s core-level spectra of BE-S and AF-S have similarities and have a difference. There are two main observable peaks at 531.35 eV (BE-S) and at 531.39 eV (AF-S) and at 532.48 eV (BE-S) and at 532.61 eV (AF-S) which shows similarities and could be assigned for (C=O) acetate/quinone/pyridone[83–85] and (O–C) acetate,[83,84,86–88] respectively. In addition, the possibility of having trapped or intercalated hydroxyl anions within the structure could be considered.[60,89,90] The difference is that there are two more peaks observed for AF-S, which appear at 530.1 and 533.9 eV. These peaks could be attributed to some adsorbed/intercalated oxygen[89,91] and N–O species.[88,92] Hence it should be assumed that, during H_2O_2 decomposition process, there is a likelihood of oxidation of some pyridinic nitrogen leading to the formation of the corresponding N-oxides.[93–95] This hypothesis supports the previous discussion about N 1s peak considering oxidized N (pyridine-N-oxide).

3.2 Decomposition of H_2O_2 and degradation of MO

Fig. 4(A) shows the dark-condition decomposition rate of H_2O_2 ($C_0 = 0.5$ mM) by Co/Zn-ZIF-8. A gradual yet rapid decrease of H_2O_2 concentration is quite observable which signifies the likely catalytic affinity of Co/Zn-ZIF-8 towards H_2O_2 decomposition. It is important to mention that without Co/Zn-ZIF-8, the dark-condition decomposition rate of H_2O_2 is limited. The heterogeneous catalytic decomposition of H_2O_2 usually obeys a pseudo-first-order kinetic model with respect to H_2O_2 regarding in-excess catalyst.[96] The known integrated form of decomposition rate equation is given as follow:

$$\ln\frac{[H_2O_2]}{[H_2O_2]_0} = -k_{dec}t$$

where k_{dec} is the H_2O_2 decomposition rate constant, t is the reaction time, $[H_2O_2]_0$ and $[H_2O_2]$ are the initial concentration and the concentration of H_2O_2 at any time t. Fig. 4(B) shows the pseudo-first-order plot of H_2O_2 decomposition by Co/Zn-ZIF-8. Linear fitting ($R^2 = 0.976$) revealed the decomposition rate constant, $k_{dec} = 0.065$ min^{-1}. In comparison to some studied catalysts of different types, Table 2, Co/Zn-ZIF-8/H_2O_2 system is competitive. To elucidate the catalytic influence of Co/Zn-ZIF-8 towards H_2O_2, the turnover number (TON) and turnover frequency (TOF) were calculated and found to be 2350 and 2820 h^{-1} respectively.

3.3 Degradation of MO

Fig. 5(A, B, and C) shows the degradation rates of MO, with initial concentrations 2, 5, and 10 ppm respectively, compared to degradation rates under conditions other than catalyst with H_2O_2. For all applied initial concentrations, degradation rates for catalyst with H_2O_2 are remarkably faster than: catalyst only, H_2O_2 only, and under vis. light solely. This designates Co/Zn-ZIF-8/H_2O_2 system as a successful system for MO degradation. Fig. 5(D) shows the effect of catalyst dose on MO degradation rate. It is obvious that as dose increases, degradation rate increases, and this is expected due to the increase of available catalyst's active sites.

Degradation rates of the different initial concentrations of MO were modelled applying a pseudo-first-order equation. This equation is similar to the previous one and is as follows:

$$\ln\frac{[MO]}{[MO]_0} = -k_{deg}t$$

where k_{deg} is the MO degradation rate constant, t is the reaction time, $[MO]_0$ and $[MO]$ are the initial concentration and the concentration of MO at any time t. Fig. 6(A–C) shows the pseudo-first-order plots of MO degradation by Co/Zn-ZIF-8/H_2O_2 system together with H_2O_2 only. Linear fittings ($R^2 \geq 0.950$) reveal the obedience of MO degradations to this model which elucidate the apparent sole dependence of degradation on MO for the applied concentration range (2–10 ppm). This behaviour suggests the possibility of treating higher MO concentrations and could imply a pure chemical process.[98]

Values of rate constants, k_{deg}, are given in Table 3. Form the table, first: MO degradation by Co/Zn-ZIF-8/H_2O_2 system is

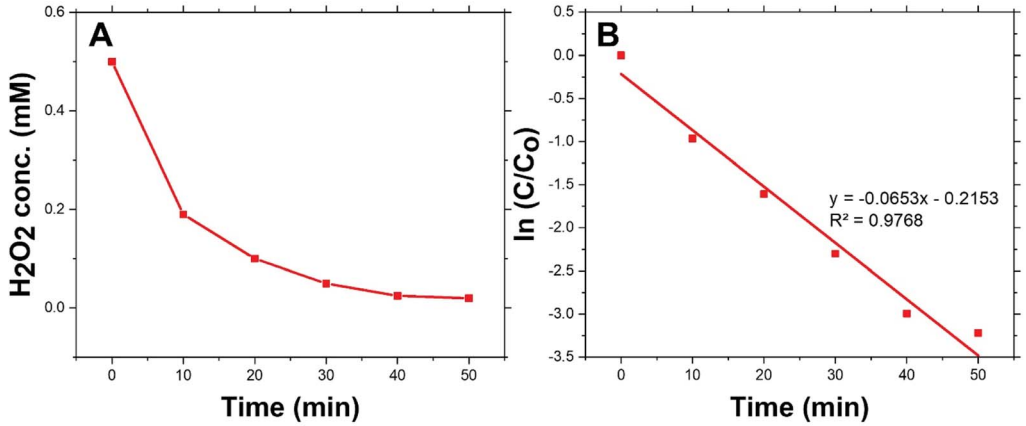

Fig. 4 (A) Decomposition of H_2O_2 over 0.05 g Co/Zn-ZIF-8 catalyst, and (B) pseudo-first-order kinetics of H_2O_2 decomposition.

Table 2 Decomposition rate constants of H_2O_2 by Co/Zn-ZIF-8 and some other selected catalysts

Material	k_{dec} (s^{-1})	References
HfO_2	$(4.3 \pm 0.9) \times 10^{-4}$	96
CDots/g-C_3N_4	7.16×10^{-4}	20
Co/Zn-ZIF-8	1.1×10^{-3}	This work
Fe_3O_4 NPs	3.94×10^{-2}	97

considerably more effective than by H_2O_2 solely with an average rate constant about 5 times that of without catalyst, second: k_{deg} values are similar to an acceptable extent, *i.e.* k_{deg} does not change with MO initial concentration, and hence one effective decomposition/degradation mechanism can be suggested, and third: k_{deg} values for Co/Zn-ZIF-8/H_2O_2 system are of the same order of k_{dec}, where $k_{deg}/k_{dec} \approx 0.65$. This ratio means that the suitable in-excess amount of degrading radicals (not too much

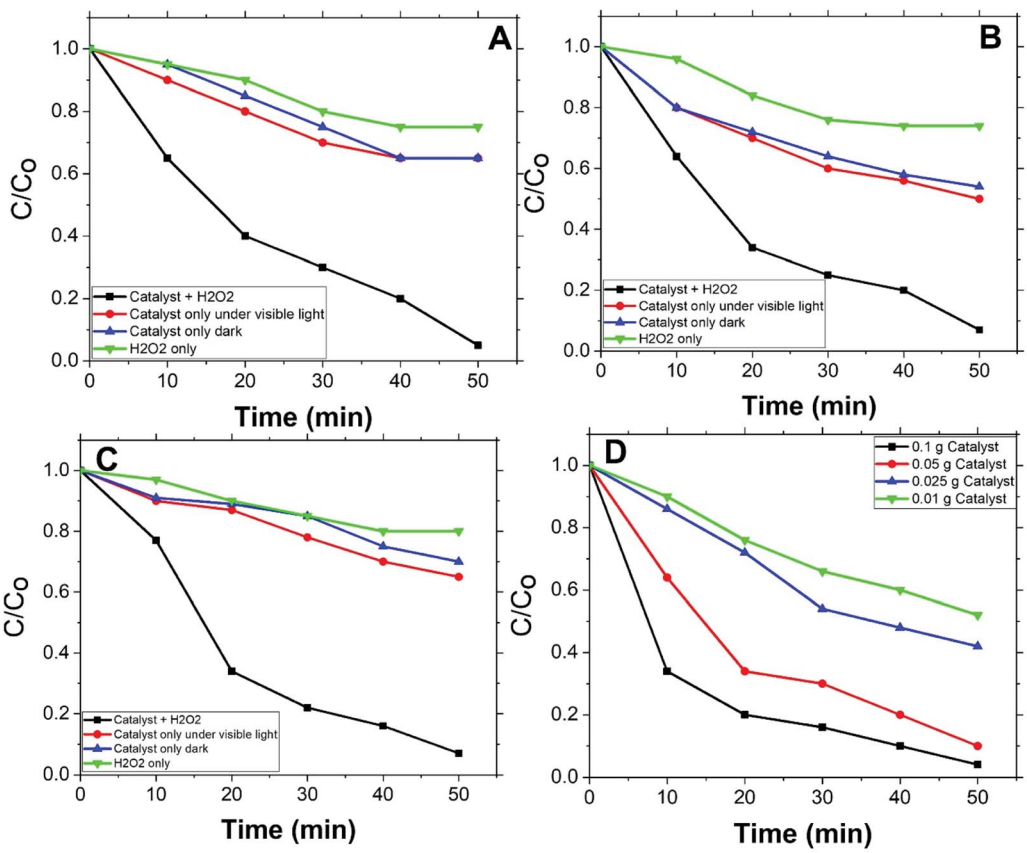

Fig. 5 MO degradation at different initial concentrations (0.05 g catalyst, 0.5 mM H_2O_2), (A) 2 ppm, (B) 5 ppm, (C) 10 ppm, and (D) degradation of 5 ppm MO at different catalyst does (0.01, 0.025, 0.05, 0.10 g).

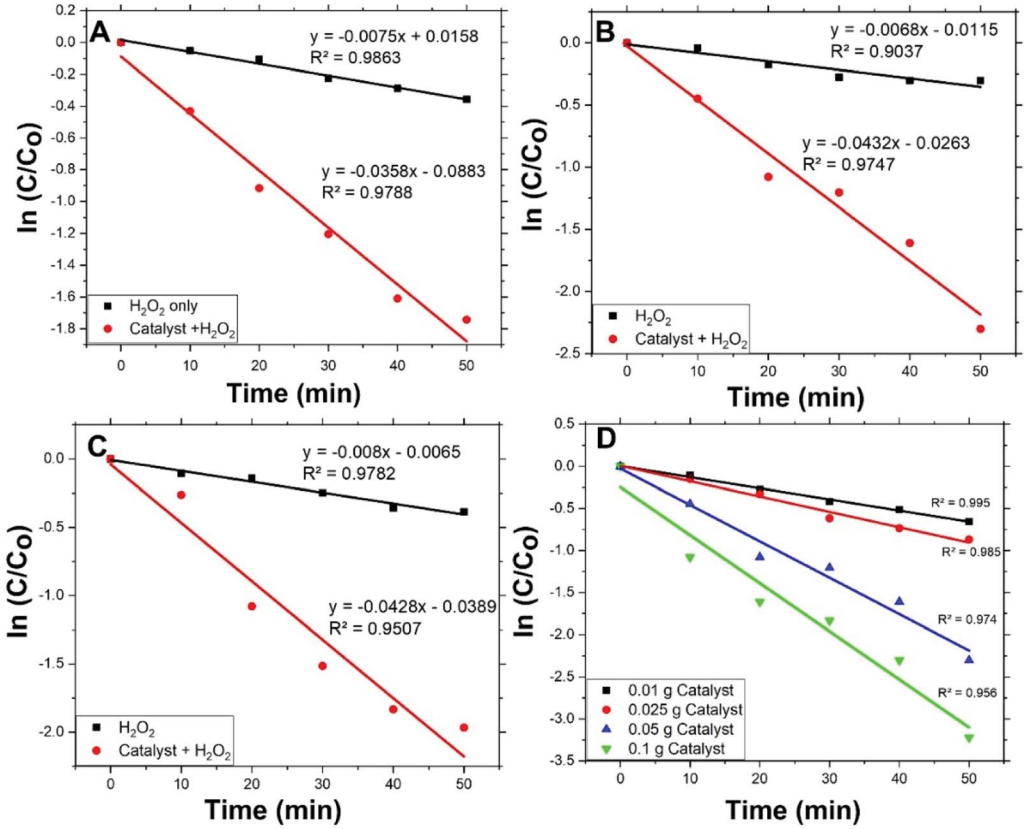

Fig. 6 Fitting of pseudo-first-order equation for MO degradation at different initial concentrations (A) 2 ppm, (B) 5 ppm, (C) 10 ppm, and (D) different dose of Co/Zn-ZIF-8 (5 ppm).

or less) should be always sufficient for continual degradation of the applied dye concentration. The adjustment of this ratio influences the efficiency and economy of the catalytic decomposition process of dyes and should be taken into consideration, *i.e.*, adjusting applied conditions to have k_{dec} value properly higher than k_{deg}.

It is important to also mention that in an investigatory preliminary experiment, mixing of MO solution and Co/Zn-ZIF-8 did not present any significant decrease in MO concentration, for about three hours, which indicates no degradation without H_2O_2 and even no observable adsorption. Hence k_{deg} can be sought catalysis-intrinsic behaviour rather than apparent and that a pure chemical process is responsible for degradation.

Another imperative observation, it has been elucidated previously that the decomposition rate of H_2O_2 without Co/Zn-ZIF-8 is almost neglected. However, MO degradation rate using H_2O_2 without Co/Zn-ZIF-8 is measurable as given in Table 3, k_{deg} = 0.007 min^{-1} on average. This suggests the importance of radical consumption, due to dye degradation, to draw further H_2O_2 decomposition.

Fig. 6(D) shows pseudo-first-order modelling of MO degradation for the different applied amounts of Co/Zn-ZIF-8 and Table 4 presents the corresponding k_{deg} values according to fitting. From the figure and the table, the amount of Co/Zn-ZIF-8 causes a steady increase of k_{deg} value. This signifies the inherent fervent of Co/Zn-ZIF-8 towards H_2O_2 decomposition. In addition, though, R^2 value constantly decreases with applied catalyst amount which points to a deviation from pseudo-first-order modelling obedience, and this may indicate the contribution of more than one mechanism as Co/Zn-ZIF-8 amount increases and/or the need to control the dose of Co/Zn-ZIF-8 with respect to applied H_2O_2 concentration. Table 5 gives a comparison for degradation rate constants given by Co/Zn-ZIF-8/H_2O_2 and some other selected catalysts/H_2O_2 systems which indicate Co/Zn-ZIF-8 as a useful catalyst.

Table 3 Degradation rate constants of MO by Co/Zn-ZIF-8/H_2O_2 and H_2O_2

$[MO]_0$ (ppm)	k_{deg} (min^{-1}) Co/Zn-ZIF-8/H_2O_2	R^2	k_{deg} (min^{-1}) H_2O_2	R^2
2	0.035	0.978	0.007	0.986
5	0.043	0.974	0.006	0.903
10	0.042	0.950	0.008	0.978

Table 4 Degradation rate constants of MO by Co/Zn-ZIF-8/H_2O_2 with different Co/Zn-ZIF-8 doses

Co/Zn-ZIF-8 (g)	k_{deg} (min^{-1}) Co/Zn-ZIF-8/H_2O_2	R^2
0.010	0.013	0.995
0.025	0.018	0.985
0.050	0.043	0.974
0.100	0.057	0.956

4. Radical scavenging experiments and reusability

In general, $^{\bullet}OH$ and $HO_2^{\bullet}$ radicals are known as the key active type in the catalytic oxidation process. $^{\bullet}OH$, radical is a strong oxidant for many organic molecules. 2-Propanol and 1,4-benzoquinone (BQ) are known as $^{\bullet}OH$ and $HO_2^{\bullet}$ scavengers respectively.[103–105] These scavengers were introduced into the reaction medium to capture $^{\bullet}OH$ and $HO_2^{\bullet}$ during the MO degradation process. The results are illustrated in Fig. 7 and point out that the addition of scavengers causes a sharp decrease in the degradation of MO from 96% to 3.5, and 6% in the presence of 2-propanol, and BQ respectively. According to the above results, it is furthermore established that the degradation of MO is mainly dependent on the availability of $^{\bullet}OH$ and $HO_2^{\bullet}$ radical species.

The reusability of a catalyst is important to consider of any heterogeneously catalyzed reaction. However, only limited experiments are there considering the reusability of powder photocatalysts in the powder form. This may be due to the difficulty in the separation of the catalyst powder after degradation processes. In the present case, it is simple to separate Co/Zn-ZIF-8 catalyst from the degradation solutions either by centrifugation or even by simple filtration. Regeneration of the catalyst was done after each dye-removal experiment, by centrifugation at 6000 rpm for 30 min, washing with water, drying at 120 °C, for 2 hours. The catalytic activity of Co/Zn-ZIF-8 remains efficient even up to 6 consecutive experiments, as depicted in Fig. 7(B), under the selected applied conditions. The remarkable stability of Co/Zn-ZIF-8 in water, as shown in the XRD patterns, sustains the chance for its reusability.

5. Proposed mechanisms of H_2O_2 decomposition

For the present work, it is important to mention the following: (i) Zn-based ZIF-8 has also been synthesized and has been applied for decomposing H_2O_2, as a supporting auxiliary experiment, however, no measurable H_2O_2-decomposition was recorded and accordingly, it can be concluded that the sole presence of Zn(II) in the nodes does not intrinsically contribute in H_2O_2 catalytic decomposition by either radical mechanism or redox mechanism, (ii) the quenching experiments revealed that

Table 5 Degradation rate constants of MO by Co/Zn-ZIF-8/H_2O_2 and some other dyes by some other selected catalysts

Catalyst	Dye	k_{deg} (s^{-1})	References
Co/Zn-ZIF-8	Methyl orange	6.7×10^{-4} (average)	This work
Copper (II)-benzoic acid complex	Methyl orange	1.1×10^{-3}	99
Natural chromite	Congo red	8.3×10^{-4} (with UV)	100
RGO	Orange II	1.3×10^{-3}	101
(MMTK10-Cu(en)$_2$)	Acid blue 29	3.233×10^{-3}	102

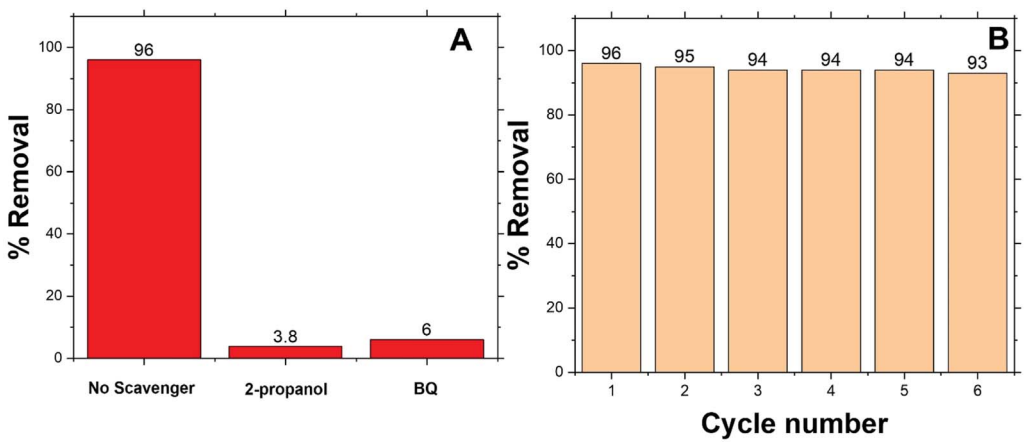

Fig. 7 (A) Quenching experiment of the active species during catalytic degradation of MO (5 ppm) over Co/Zn-ZIF-8, 0.5 mM H_2O_2, with the addition of methanol, ethanol and 2-propanol as scavengers for $^{\bullet}OH$, (B) 6-cycle reuse of Co/Zn-ZIF-8, 0.05 mM H_2O_2 in the degradation of MB (initial pH 6.5, 5 ppm).

˙OH is the main formed radical upon H_2O_2 decomposition and hence being responsible for dye-degradation, and (iii) no significant change of pH value was recorded.

Hence, the proposal of H_2O_2-decomposition over Co/Zn-ZIF-8 is based on the following suppositions: (i) nodes of Co/Zn-ZIF-8 are sought as nitrides moieties, zinc nitride and cobalt nitride, (ii) these metal nitrides are very similar to metal oxides, because of the very similarity of electronegativity of nitrogen and oxygen, (iii) cobalt-nods are the active sites at which H_2O_2-decomposition takes place (due to possible redox), and (iv) hydrogen bonding of H_2O_2 with nitrogen (replacing some hydrogen-bonded H_2O) can cause accumulation of H_2O_2 onto catalyst surface and then a stronger interaction can cause adsorption of H_2O_2 with zinc nitride and cobalt nitride moieties (similar to oxides) by the interaction of its O atoms with the surface metal cations leading to a strong type of interaction.[96]

Fig. 8 shows the EPR patterns (range: 310–370 mT) for BE-S and AF-S. Comparison of AF-S pattern with respect to that of BE-S, confirms the presence of free radicals after H_2O_2 treatment as it shows six characteristic peaks corresponding to the Zn^{2+} and Co^{2+} catalytic centers within Co/Zn-ZIF-8 to produce free radicals *via* electron transfer upon treating the Co/Zn-ZIF-8 with hydrogen peroxide. In some previous works, EPR/ESR measurements revealed the presence of ˙OH and HO_2˙ species on the surface of different oxides catalysts. These species are normally short-lived and reactive, however, they become long-lived because of the enhanced stabilization due to their adsorption onto the oxide surface.[106]

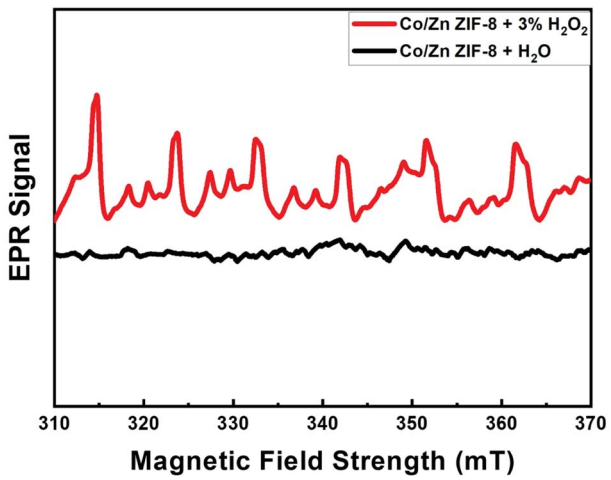

Fig. 8 EPR signal of Co/Zn-ZIF-8.

Decomposition of hydrogen peroxide on a solid surface is a spontaneous process at temperatures that range from room temperature to 286 °C. In addition, it was revealed that energy barrier for reactions catalyzed by surface sites where the metal atoms are of under-coordination should be lower than the energy barrier for equivalent reactions catalyzed by non-defected surfaces.[106] Two possible mechanisms can be given as follows:

(1) The first (radical mechanism) is based on the complexation of H_2O_2 with catalyst surface where H_2O_2 coordinates with surface-metal followed by a series of surface reactions leading, eventually, to the decomposition of H_2O_2 into the oxidizing radicals, ˙OH and HO_2˙:[107,108]

(I) Being in an aqueous medium, adsorption of H_2O preponderates the ZIF-surface. Continual coordination-adsorption of H_2O_2 molecules onto ZIF-surface occurs *via* replacing some H_2O molecules where coordinated H_2O_2 suffers decomposition. This repeated adsorption step grantees the continuous-controlled consumption of H_2O_2:

$$[H_2O_{ads}\text{–}Co(II)]_s + H_2O_2 \leftrightarrow [H_2O_{2ads}\text{–}Co(II)]_s + H_2O$$

(II) Decompositions of H_2O_2 and desorption of radicals:

$$[H_2O_{2ads}\text{–}Co(II)]_s \leftrightarrow [HO^{\bullet}\text{–}Co(II)]_s + \mathbf{^{\bullet}OH} \text{ (homolytic)}$$

$$[H_2O_{2ads}\text{–}Co(II)]_s \leftrightarrow [HO_2^{\bullet}\text{–}Co(II)]_s + \mathbf{^{\bullet}H} \text{ (heterolytic)}$$

$$[HO_2^{\bullet}{}_{ads}\text{–}Co(II)]_s \leftrightarrow \text{–}Co(II) + \mathbf{HO_2^{\bullet}}$$

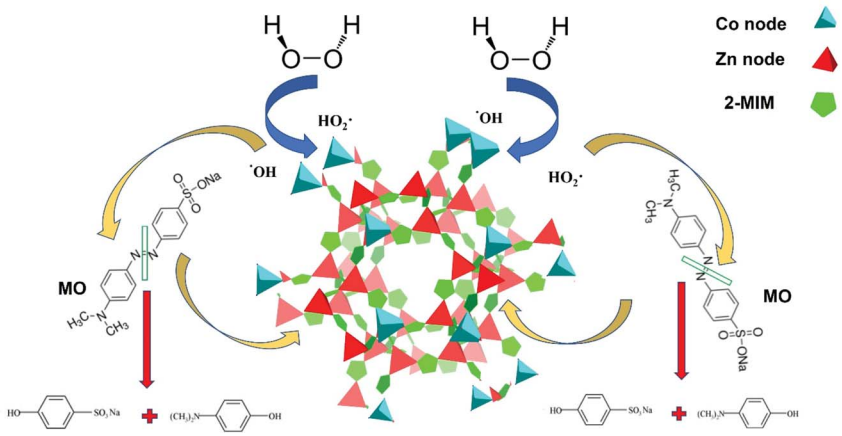

Fig. 9 Schematic illustration of the proposed redox mechanism of H_2O_2 decomposition by Co/Zn-ZIF-8 catalyst and the subsequent MO degradation.

In this mechanism, Co(III) nodes may contribute to the decomposition process likewise Co(II).

(2) The second (redox mechanism) is analogous to the Haber–Weiss mechanism albeit with a metal ion belongs to solid surface:[109]

$$[H_2O_{ads}\text{–}Co(II)]_s + H_2O_2 \leftrightarrow [H_2O_{2ads}\text{–}Co(II)]_s + H_2O \quad (1)$$

$$[H_2O_{2ads}\text{–}Co(II)]_s + H_2O \rightarrow [H_2O_{ads}\text{–}Co(III)]_s + \mathbf{^{\cdot}OH} + OH^- \quad (2)$$

$$[H_2O_{ads}\text{–}Co(III)]_s + H_2O_2 \rightarrow [H_2O_{2ads}\text{–}Co(III)]_s + H_2O \quad (3)$$

$$[H_2O_{2ads}\text{–}Co(III)]_s + H_2O \rightarrow [H_2O_{ads}\text{–}Co(II)]_s + \mathbf{HO_2^{\cdot}} + H^+ \quad (4)$$

Monitoring of pH during decomposition did not give a significant change which suggests similar rates of both the eqn (2) and (4) where a balance occurs for the formation of OH^- and H^+. Hence, the catalytic overall decomposition reaction, *via* Co(II)/Co(III) redox consecutive cyclic process, should be:

$$2H_2O_2 \rightarrow +\mathbf{HO_2^{\cdot}} + \mathbf{^{\cdot}OH} + H_2O \quad (5)$$

Herein, Co(III) nodes essentially contribute to the decomposition process by forming a redox pair with Co(II), *i.e.* Co(II)/Co(III) redox system.

Both stability of pH and the previously discussed XPS analysis, which revealed that cobalt ions of different coordination environments and different oxidation states permit the consecutive redox reaction suggesting a redox mechanism to predominate the decomposition process (Fig. 9).

6. Conclusions

The successful synthesis of Co/Zn-ZIF-8 in an aqueous medium points to the importance of zinc nodes to stabilize the material against hydro-chemical stress. Detailed study of XPS patterns of a hybrid material before and after catalysis is a strong tool to disclose some verities about the changes that happened within the material structure and the function(s) of its compositions. For Co/Zn-ZIF-8, XPS detailed analysis made known the importance of the mixed oxidation of cobalt for H_2O_2 redox decomposition. For Co/Zn-ZIF-8, H_2O_2-decomposition rate constant, k_{dec}, and the average MO-degradation rate constant, k_{deg}, were found of the same order, where $k_{deg}/k_{dec} \approx 0.65$. Hence, regulating degradation conditions, specifically H_2O_2 and dye concentration and catalyst amount, is important for the appropriate decomposition/degradation process.

Conflicts of interest

There are no conflicts to declare.

References

1 J. K. Zareba, M. Nyk and M. Samoć, *Cryst. Growth Des.*, 2016, **16**, 6419–6425.
2 K. Zhou, B. Mousavi, Z. Luo, S. Phatanasri, S. Chaemchuen and F. Verpoort, *J. Mater. Chem. A*, 2017, **5**, 952–957.
3 O. Abuzalat, D. Wong, S. S. Park and S. Kim, *Nanoscale*, 2020, **12**, 13523–13530.
4 B. Chen, Z. Yang, Y. Zhu and Y. Xia, *J. Mater. Chem. A*, 2014, **2**, 16811–16831.
5 S.-G. Jeon, J.-W. Ko and W.-B. Ko, *Catalysts*, 2021, **11**, 1022.
6 T. N. Nguyen, H. P. Nguyen, T.-H. Kim and S. W. Lee, *Korean J. Mater. Res.*, 2018, **28**, 68–74.
7 M. Zhu, D. Srinivas, S. Bhogeswararao, P. Ratnasamy and M. A. Carreon, *Catal. Commun.*, 2013, **32**, 36–40.
8 P.-Z. Li, K. Aranishi and Q. Xu, *Chem. Commun.*, 2012, **48**, 3173–3175.
9 C. M. Miralda, E. E. Macias, M. Zhu, P. Ratnasamy and M. A. Carreon, *ACS Catal.*, 2012, **2**, 180–183.
10 Y. Guan, J. Shi, M. Xia, J. Zhang, Z. Pang, A. Marchetti, X. Wang, J. Cai and X. Kong, *Appl. Surf. Sci.*, 2017, **423**, 349–353.
11 L. T. Nguyen, K. L. Ky and T. Nam, *Chin. J. Catal.*, 2012, **33**, 688–696.
12 C. Chizallet, S. Lazare, D. Bazer-Bachi, F. Bonnier, V. Lecocq, E. Soyer, A.-A. Quoineaud and N. Bats, *J. Am. Chem. Soc.*, 2010, **132**, 12365–12377.
13 L. H. Wee, T. Lescouet, J. Ethiraj, F. Bonino, R. Vidruk, E. Garrier, D. Packet, S. Bordiga, D. Farrusseng and M. Herskowitz, *ChemCatChem*, 2013, **5**, 3562–3566.
14 S. Chirra, L.-F. Wang, H. Aggarwal, M.-F. Tsai, S. S. Soorian, S. Siliveri, S. Goskula, S. R. Gujjula and V. Narayanan, *Mater. Today Commun.*, 2021, **26**, 101993.
15 S. Radoor, J. Karayil, A. Jayakumar, J. Parameswaranpillai and S. Siengchin, *Colloids Surf., A*, 2021, **611**, 125852.
16 J. Wei, D. Zhang, L. Zhang, H. Ouyang and Z. Fu, *ACS Appl. Mater. Interfaces*, 2019, **11**, 35597–35603.
17 H. Hatem, M. S. El-Geundi, H. Tantawy and A. Baraka, *J. Solid State Chem.*, 2020, **286**, 121271.
18 M. Mohsen, I. Naeem, M. Awaad, H. Tantawy and A. Baraka, *J. Solid State Chem.*, 2020, **289**, 121493.
19 C. Hochanadel, *J. Phys. Chem.*, 1952, **56**, 587–594.
20 Z. Liu, Q. Shen, C. Zhou, L. Fang, M. Yang and T. Xia, *Catalysts*, 2018, **8**, 445.
21 O. Karagiaridi, M. B. Lalonde, W. Bury, A. A. Sarjeant, O. K. Farha and J. T. Hupp, *J. Am. Chem. Soc.*, 2012, **134**, 18790–18796.
22 N. Nagarjun and A. Dhakshinamoorthy, *New J. Chem.*, 2019, **43**, 18702–18712.
23 T. Ivanova, A. Naumkin, A. Sidorov, I. Eremenko and M. Kiskin, *J. Electron Spectrosc. Relat. Phenom.*, 2007, **156**, 200–203.
24 M. Fantauzzi, F. Secci, M. S. Angotzi, C. Passiu, C. Cannas and A. Rossi, *RSC Adv.*, 2019, **9**, 19171–19179.
25 P. Shelke, Y. Khollam, K. Patil, S. Gunjal, S. Jadkar, M. Takwale and K. Mohite, *J. Nano- Electron. Phys.*, 2011, **3**, 486.
26 C. Vaz, D. Prabhakaran, E. Altman and V. Henrich, *Phys. Rev. B: Condens. Matter Mater. Phys.*, 2009, **80**, 155457.
27 Q. Duan and H. Chen, *IOP Conf. Ser.: Mater. Sci. Eng.*, 2017, **207**(1), 012020.

28 D. G. Brown and U. Weser, *Z. Naturforsch., B: J. Chem. Sci.*, 1979, **34**, 1468–1470.
29 N. Alotaibi, H. H. Hammud, R. K. Karnati, S. G. Hussain, J. Mazher and T. Prakasam, *RSC Adv.*, 2020, **10**, 17660–17672.
30 Y. Yang, Y. Tu, P. Zhu, L. Zhang, T. Li, H. Zheng, R. Sun and C. Wong, *Sustainable Energy Fuels*, 2018, **2**, 2345–2357.
31 C. Li, Q. Yang, M. Shen, J. Ma and B. Hu, *Energy Storage Mater.*, 2018, **14**, 82–89.
32 Z. Jiang, Z. Li, Z. Qin, H. Sun, X. Jiao and D. Chen, *Nanoscale*, 2013, **5**, 11770–11775.
33 A. Gabe, J. García-Aguilar, Á. Berenguer-Murcia, E. Morallón and D. Cazorla-Amorós, *Appl. Catal., B*, 2017, **217**, 303–312.
34 N. Osenciat, D. Bérardan, D. Dragoe, B. Leridon, S. Holé, A. K. Meena, S. Franger and N. Dragoe, *J. Am. Ceram. Soc.*, 2019, **102**, 6156–6162.
35 B. J. Tufts, I. L. Abrahams, C. E. Caley, S. R. Lunt, G. M. Miskelly, M. J. Sailor, P. G. Santangelo, N. S. Lewis, A. L. Roe and K. O. Hodgson, *J. Am. Chem. Soc.*, 1990, **112**, 5123–5136.
36 T. J. Chuang, C. R. Brundle and D. W. Rice, *Surf. Sci.*, 1976, **59**, 413–429.
37 E. Meza, J. Ortiz, D. Ruíz-León, J. F. Marco and J. L. Gautier, *Mater. Lett.*, 2012, **70**, 189–192.
38 Y. Duan, T. Hu, L. Yang, J. Gao, S. Guo, M. Hou and X. Ye, *J. Alloys Compd.*, 2019, **771**, 156–161.
39 M. Bravo Sanchez, J. A. Huerta-Ruelas, D. Cabrera-German and A. Herrera-Gomez, *Surf. Interface Anal.*, 2017, **49**, 253–260.
40 W. Xi, G. Yan, Z. Lang, Y. Ma, H. Tan, H. Zhu, Y. Wang and Y. Li, *Small*, 2018, **14**, 1802204.
41 J. Janas, J. Gurgul, R. P. Socha, T. Shishido, M. Che and S. Dzwigaj, *Appl. Catal., B*, 2009, **91**, 113–122.
42 T. Zhou, Z. Cao, H. Wang, Z. Gao, L. Li, H. Ma and Y. Zhao, *RSC Adv.*, 2017, **7**, 22818–22824.
43 Q. Zhang, H. Chen, X. Han, J. Cai, Y. Yang, M. Liu and K. Zhang, *ChemSusChem*, 2016, **9**, 186–196.
44 P. Srinivasan, A. J. Kulandaisamy, G. K. Mani, K. J. Babu, K. Tsuchiya and J. B. B. Rayappan, *RSC Adv.*, 2019, **9**, 30226–30239.
45 P. W. Menezes, A. Indra, A. Bergmann, P. Chernev, C. Walter, H. Dau, P. Strasser and M. Driess, *J. Mater. Chem. A*, 2016, **4**, 10014–10022.
46 W. Guo, Z. Liang, J. Zhao, B. Zhu, K. Cai, R. Zou and Q. Xu, *Small Methods*, 2018, **2**, 1800204.
47 A. V. Piskunov, K. I. Pashanova, A. S. Bogomyakov, I. V. Smolyaninov, A. G. Starikov and G. K. Fukin, *Dalton Trans.*, 2018, **47**, 15049–15060.
48 Y. K. Penke, G. Anantharaman, J. Ramkumar and K. K. Kar, *ACS Appl. Mater. Interfaces*, 2017, **9**, 11587–11598.
49 L. Huang, D. Chen, G. Luo, Y. R. Lu, C. Chen, Y. Zou, C. L. Dong, Y. Li and S. Wang, *Adv. Mater.*, 2019, **31**, 1901439.
50 S. Dou, C.-L. Dong, Z. Hu, Y.-C. Huang, J.-l. Chen, L. Tao, D. Yan, D. Chen, S. Shen, S. Chou and S. Wang, *Adv. Funct. Mater.*, 2017, **27**, 1702546.
51 M. C. Biesinger, L. W. Lau, A. R. Gerson and R. S. C. Smart, *Appl. Surf. Sci.*, 2010, **257**, 887–898.
52 M. Vijayaraj and C. S. Gopinath, *J. Catal.*, 2006, **241**, 83–95.
53 A. K. Yadav, R. Dey, R. Bhunia, S. Hussain, S. N. Jha, D. Bhattacharyya, R. Bhar and A. K. Pal, *J. Polym. Res.*, 2016, **23**, 1–10.
54 S. Sampath, M. Shestakova, P. Maydannik, T. Ivanova, T. Homola, A. Bryukvin, M. Sillanpää, R. Nagumothu and V. Alagan, *RSC Adv.*, 2016, **6**, 25173–25178.
55 J. P. Singh, S. H. Kim, S. O. Won, W. C. Lim, I.-J. Lee and K. H. Chae, *CrystEngComm*, 2016, **18**, 2701–2711.
56 C. Chen, Z. Cao, X. Zhang, Y. Li, L. Yu and X. Jiang, *Chin. J. Chem.*, 2020, **38**, 1045–1051.
57 Z. Cao, X. Deng, C. Chen, Y. Liu, L. Yu and X. Jiang, *React. Chem. Eng.*, 2021, **6**, 454–458.
58 Y. Wang, Q. Du, H. Zhao, S. Hou, Y. Shen, H. Li, X. Kong, W. Sun, B. Zhang and S. Li, *Nanoscale*, 2018, **10**, 17958–17964.
59 H. Chen, X. Wu, R. Zhao, Z. Zheng, Q. Yuan, Z. Dong and W. Gan, *Microchim. Acta*, 2019, **186**, 1–9.
60 S. Bibi, E. Pervaiz, M. Yang and O. Rabi, *Catalysts*, 2021, **11**, 304.
61 L. Xu, F. Meng, X. Wei, C. Lin, L. Zheng and J. Liu, *Sci. China: Technol. Sci.*, 2020, **63**, 1730–1738.
62 S. Zhuang, E. S. Lee, L. Lei, B. B. Nunna, L. Kuang and W. Zhang, *Int. J. Energy Res.*, 2016, **40**, 2136–2149.
63 Y. Zhu, K. Miyake, Y. Shu, A. Gabe, Y. Hirota, Y. Uchida, S. Tanaka, E. Morallón, D. Cazorla-Amorós and N. Nishiyama, *Catal. Sci. Technol.*, 2019, **9**, 578–582.
64 Y. Jiang, Y. Lu, X. Wang, Y. Bao, W. Chen and L. Niu, *Nanoscale*, 2014, **6**, 15066–15072.
65 M. Mohsen, I. Naeem, M. I. Awaad, H. R. Tantawy and A. Baraka, *J. Solid State Chem.*, 2020, **289**, 121493.
66 C. S. Budi, J. R. Deka, W.-C. Hsu, D. Saikia, K.-T. Chen, H.-M. Kao and Y.-C. Yang, *J. Hazard. Mater.*, 2021, **407**, 124392.
67 A. Vesel, R. Zaplotnik, G. Primc and M. Mozetič, *Nanomaterials*, 2020, **10**(11), 2286.
68 W. Kiciński and S. Dyjak, *Molecules*, 2021, **26**, 668.
69 W. Ding, Z. Wei, S. Chen, X. Qi, T. Yang, J. Hu, D. Wang, L.-J. Wan, S. F. Alvi and L. Li, *Angew. Chem., Int. Ed.*, 2013, **52**, 11755–11759.
70 X. L. Wei, M. Fahlman and A. J. Epstein, *Macromolecules*, 1999, **32**, 3114–3117.
71 H. R. Tantawy, B.-A. F. Kengne, D. N. McIlroy, T. Nguyen, D. Heo, Y. Qiang and D. E. Aston, *J. Appl. Phys.*, 2015, **118**, 175501.
72 H. S. OnáChan, L. MingáGan, C. HaráChew and S. HowáSeow, *J. Mater. Chem.*, 1993, **3**, 1109–1115.
73 H. Lee, Y. N. Choi, S. B. Choi, J. H. Seo, J. Kim, I. H. Cho, S. Gang and C. H. Jeon, *J. Phys. Chem. C*, 2014, **118**, 5691–5699.
74 Y. Wu, X. Song, S. Xu, J. Zhang, Y. Zhu, L. Gao and G. Xiao, *Catal. Lett.*, 2019, **149**, 2575–2585.
75 A. Indra, P. W. Menezes, K. Kailasam, D. Hollmann, M. Schröder, A. Thomas, A. Brückner and M. Driess, *Chem. Commun.*, 2016, **52**, 104–107.

76 H. Liu, Z. Li, L. Zhang, H. Ruan and R. Hu, *Nanoscale Res. Lett.*, 2019, **14**, 1–10.
77 B. Yin, X. Cao, A. Pan, Z. Luo, S. Dinesh, J. Lin, Y. Tang, S. Liang and G. Cao, *Adv. Sci.*, 2018, **5**, 1800829.
78 S. Dorey, F. Gaston, S. R. Marque, B. Bortolotti and N. Dupuy, *Appl. Surf. Sci.*, 2018, **427**, 966–972.
79 L. Ma, X. Zhang, M. Ikram, M. Ullah, H. Wu and K. Shi, *Chem. Eng. J.*, 2020, **395**, 125216.
80 B. Ding, J. Wang, Z. Chang, G. Xu, X. Hao, L. Shen and X. Zhang, *ChemElectroChem*, 2016, **3**(4), 668–674.
81 J. P. Sousa, M. F. Pereira and J. L. Figueiredo, *Fuel Process. Technol.*, 2013, **106**, 727–733.
82 H. Sepehrmansourie, M. Zarei, M. A. Zolfigol, S. Babaee and S. Rostamnia, *Sci. Rep.*, 2021, **11**, 1–15.
83 A. Ganguly, S. Sharma, P. Papakonstantinou and J. Hamilton, *J. Phys. Chem. C*, 2011, **115**, 17009–17019.
84 Z. Xing, Z. Ju, Y. Zhao, J. Wan, Y. Zhu, Y. Qiang and Y. Qian, *Sci. Rep.*, 2016, **6**, 1–10.
85 M. P. Woods, E. J. Biddinger, P. H. Matter, B. Mirkelamoglu and U. S. Ozkan, *Catal. Lett.*, 2010, **136**, 1–8.
86 M. González-Torres, M. G. Olayo, G. J. Cruz, L. M. Gómez, V. Sánchez-Mendieta and F. González-Salgado, *Adv. Chem.*, 2014, **2014**, 1–8.
87 B. Huang, G. Liu, P. Wang, X. Zhao and H. Xu, *Processes*, 2019, **7**, 167.
88 J. L. Hueso, J. P. Espinós, A. Caballero, J. Cotrino and A. R. González-Elipe, *Carbon*, 2007, **45**, 89–96.
89 Y.-C. Cheng, S.-P. Chang, S.-J. Chang, T.-H. Cheng, Y.-L. Tsai, Y.-Z. Chiou and L. Lu, *ECS J. Solid State Sci. Technol.*, 2019, **8**, Q3034.
90 F. Gu, W. Liu, Y. Song, L.-M. Liu and Y. Zhu, *Ionics*, 2020, **26**, 5897–5906.
91 M. Scardamaglia, T. Susi, C. Struzzi, R. Snyders, G. Di Santo, L. Petaccia and C. Bittencourt, *Sci. Rep.*, 2017, **7**, 7960.
92 S. Shahriar, V. Castaneda, M. Martinez, A. K. Mishra, T. Akter, K. Schutt, J. A. Boscoboinik and D. Hodges, *J. Renewable Sustainable Energy*, 2019, **11**, 053504.
93 G. Gajeles, S. M. Kim, J.-C. Yoo, K.-K. Lee and S. H. Lee, *RSC Adv.*, 2020, **10**, 9165–9171.
94 F. F. Bamoharram, M. M. Heravi, M. Roshani and N. Tavakoli, *J. Mol. Catal. A: Chem.*, 2006, **252**, 219–225.
95 W. Xie, Y. Zheng, S. Zhao, J. Yang, Y. Liu and P. Wu, *Catal. Today*, 2010, **157**, 114–118.
96 C. M. Lousada, M. Yang, K. Nilsson and M. Jonsson, *J. Mol. Catal. A: Chem.*, 2013, **379**, 178–184.
97 A. Maharjan, P. K. Dikshit, A. Gupta and B. S. Kim, *J. Chem. Technol. Biotechnol.*, 2020, **95**, 2495–2508.
98 C. Chen, X. Zhang, H. Cao, F. Wang, L. Yu and Q. Xu, *Adv. Synth. Catal.*, 2019, **361**, 603–610.
99 H. Sun and Z. Zhang, *J. Chem. Eng. Jpn.*, 2017, **50**, 26–30.
100 M. Shaban, M. R. Abukhadra, S. S. Ibrahim and M. G. Shahien, *Appl. Water Sci.*, 2017, **7**, 4743–4756.
101 S. D. Ovhal, C. S. Rodrigues and L. M. Madeira, *J. Chem. Technol. Biotechnol.*, 2021, **96**, 349–359.
102 I. A. Salem, H. A. El-Ghamry and M. A. El-Ghobashy, *Beni Suef Univ. J. Basic Appl. Sci.*, 2014, **3**, 186–192.
103 O. Abuzalat, H. Tantawy, R. Abdlaty, M. Elfiky and A. Baraka, *Dalton Trans.*, 2021, **50**(24), 8600–8611.
104 X. Wang, M. Brigante, W. Dong, Z. Wu and G. Mailhot, *Chemosphere*, 2020, **258**, 127268.
105 M. Sadeghi, S. Farhadi and A. Zabardasti, *RSC Adv.*, 2020, **10**, 10082–10096.
106 C. M. Lousada, A. J. Johansson, T. Brinck and M. Jonsson, *J. Phys. Chem. C*, 2012, **116**, 9533–9543.
107 X.-j. Yang, P.-f. Tian, H.-l. Wang, J. Xu and Y.-f. Han, *J. Catal.*, 2016, **336**, 126–132.
108 M. Sadeghi, S. Farhadi and A. Zabardasti, *RSC Adv.*, 2020, **10**, 44034–44049.
109 K. Rusevova, F.-D. Kopinke and A. Georgi, *J. Hazard. Mater.*, 2012, **241**, 433–440.